

High- z Ly α Emitters. I. A Blank-Field Search for Objects Near Redshift $z = 3.4$ in and around the Hubble Deep Field and the Hawaii Deep Field SSA22¹

Lennox L. Cowie^{2,3} and Esther M. Hu²

Institute for Astronomy, University of Hawaii, 2680 Woodlawn Drive, Honolulu, HI 96822
 cowie@ifa.hawaii.edu, hu@ifa.hawaii.edu

ABSTRACT

We present deep narrow-band ($\lambda = 5390 \text{ \AA}$, $\Delta\lambda = 77 \text{ \AA}$) and multi-color observations of the Hubble Deep Field and the Hawaii Deep Field SSA22 obtained with the LRIS instrument at the Keck II 10-m telescope. It is shown that there is a substantial population of galaxies at $z \sim 3.4$ which can be selected by Ly α emission. Comparison with color-selected samples shows that the samples selected with these different criteria have substantial, but not complete overlap, and that there is a comparable surface density in the two selected populations. The emission-line selected samples include objects with strong Ly α , and which are significant contributors to the integrated star formation at these epochs. For a Salpeter IMF we estimate a minimum star formation rate of $0.01 M_{\odot} \text{ Mpc}^{-3} \text{ yr}^{-1}$ at $z = 3.4$ for $H_0 = 65 \text{ km s}^{-1} \text{ Mpc}^{-1}$ and $q_0 = 0.5$ in the Ly α -selected objects, though the value could be substantially higher if there is significant extinction.

Subject headings: cosmology: early universe — cosmology: observations — galaxies: evolution — galaxies: formation

¹Based in part on observations with the NASA/ESA *Hubble Space Telescope* obtained at the Space Telescope Science Institute, which is operated by AURA, Inc., under NASA contract NAS 5-26555.

²Visiting Astronomer, W. M. Keck Observatory, jointly operated by the California Institute of Technology, the University of California, and the National Aeronautics and Space Administration.

³Visiting Astronomer, Canada-France-Hawaii Telescope, operated by the National Research Council of Canada, the Centre National de la Recherche Scientifique of France, and the University of Hawaii.

1. Introduction

Recent opinion has swung heavily to the viewpoint that emission-line searches for high- z Ly α emitters have failed, and that color-based searches may represent the only realistic way to identify high-redshift galaxies. In the present series of papers we shall show that this assumption is ill-founded and that slightly more sensitive searches than previously carried out yield very large numbers of high- z Ly α emitters, including some objects which are so faint in the continuum that they would not be easily detected on the basis of their colors. The results show that emission-line searches using 10-m class telescopes and either narrow-band or spectroscopic techniques are an efficient means of identifying and studying the distribution and clustering of high-redshift galaxies, including objects beyond redshift 5.

Indeed, the pessimism has not been justified even based on existing data. Surveys around known objects have yielded numbers of Ly α emitters both at moderate z (Djorgovski *et al.* 1985; Macchetto *et al.* 1993; Francis *et al.* 1996; Pascarelle *et al.* 1996; Djorgovski *et al.* 1996; Francis *et al.* 1997) and high z (Hu *et al.* 1996; Petitjean *et al.* 1996; Hu & McMahon 1996; Hu *et al.* 1997), and while these results may be dismissed as a consequence of the possibly anomalous environments around the target objects, it is also true that quite a large fraction of the color-selected $z = 2 \rightarrow 4$ objects have Ly α in emission (cf. Steidel *et al.* 1996a, 1996b; Lowenthal *et al.* 1997; Steidel *et al.* 1998). Indeed, these latter results show at once that blank field objects can be found with only a small increase in sensitivity over the existing Ly α surveys summarized by Pritchet (1994).

A substantial gain in depth is now possible with the advent of the 10-m telescopes, and in order to exploit this we have begun a narrow-band filter search for high- z Ly α emitters using the LRIS instrument (Oke *et al.* 1995) in imaging mode on the Keck II 10-m telescope with specially designed filters. In the present paper we describe observations of a 25.3 \square' region surrounding the Hubble Deep Field (HDF) (Williams *et al.* 1996) and a similar area around the Hawaii Deep Field SSA22 (Cowie *et al.* 1994) in broad-band B , V , and I colors, and using a filter centered at 5390 Å which covers a 77 Å bandpass. This filter would detect Ly α at $z = 3.405 \rightarrow 3.470$. Subsequent papers in this series will address deep slit spectroscopy of quasar and blank fields, and deep optical and infrared narrow-band imaging studies at higher redshifts. At the time of the filter design no objects were known to lie within the filter redshift range, but subsequently one such object was identified by Lowenthal *et al.* (1997) in the HDF field itself. The search is therefore a blank-field search, but among the objects identified as Ly α emitters in this redshift interval, the survey does indeed recover the $z = 3.430$ object found by Lowenthal *et al.* (identified as hd2-0698-1297 in their paper).

SSA22 and the HDF are ideal test areas for a narrow-band imaging search because of the large number of spectroscopic redshift identifications in and around these areas and the

ultra-deep multicolor photometric information available in the HDF proper. Thus a survey using these fields allows us to address issues such as: (1) comparing methodologies and sensitivities of narrow-band emission-line techniques and continuum color-break techniques for identifying high-redshift galaxies, (2) determining relative numbers of foreground emission-line objects and determining the best methods for distinguishing between the various types of emitters (*e.g.*, Ly α , [O II], H β , [O III]), (3) estimating the relative surface density of high-redshift candidates as a function of flux found using each technique, and (4) establishing a baseline for comparison between blank-field and targeted searches around high- z objects (such as radio galaxies, DLAs, and quasars), and for evolution of galaxy properties at higher redshifts. In addition, we can establish specified criteria (*e.g.*, desired magnitude limits, required precision of color estimates for separating objects of different redshift, typical spatial extents) on well-studied fields with high-resolution images, which then permits fine-tuning future investigations of high-redshift galaxies. Finally, when used in conjunction with optical and infrared narrow-band surveys currently in progress, the incidence and statistics of foreground emission-line objects are also of interest for estimating the surface densities of star-forming galaxies and AGN at different epochs, and for comparing indices such as [O II] with primary star-formation indices such as H α (Kennicutt 1983, 1992) or the far UV flux, in order to track the evolution of star formation history to very high redshifts. We shall address these issues in subsequent papers.

2. Data

Narrow-band observations using the LRIS camera were obtained on the Hubble Deep Field (HDF) on the night of UT 1997 May 2 and on SSA22 on the nights of UT 1997 August 8 and 10. The narrow-band filter was a specially designed 9''5 square interference filter centered at 5390 Å, with a peak transmission of just under 70% and FWHM of 77 Å, and located in the collimated beam at the standard LRIS filter position. The filter lies in a very dark region of sky and was also matched to a dark portion of the IR sky where [O II] would lie if Ly α were in the optical narrow-band. For the HDF a series of 900-sec exposures (2 hrs) shifted by 15'' between successive frames were taken in the narrow-band filter, immediately followed by a series of 360-sec V -band exposures (0.6 hrs) on the same field. These data were combined with a series of 420-sec B -band exposures (0.7 hrs) taken with LRIS on the night of UT 1997 March 8. For SSA22 a 5 hr narrow-band exposure was taken, again as a series of 900-sec exposures, while the B data were acquired as a series of 420-sec exposures (0.8 hrs) on UT 1997 August 9, with the V data taken as a series of 400-sec exposures over the nights of UT 1997 August 8 and 10 (1.6 hrs), and I data taken as a series of 300-sec exposures on UT 1997 August 10 (0.7 hrs). The data were processed using median sky flats

generated from the dithered images and calibrated using observations of Landolt standard stars (Landolt 1992) and spectrophotometric standards (Massey *et al.* 1988). The FWHM is $\sim 0''.7$ on all the composite images, which were obtained under photometric conditions, and for the HDF the narrow-band reaches a 1σ limiting AB magnitude of 26.8 in a $3''$ diameter aperture, corrected to a total magnitude following the procedures of Cowie *et al.* (1994). The corresponding 1σ flux limit is 6×10^{-18} erg cm $^{-2}$ s $^{-1}$ over a $3''$ diameter aperture. For SSA22 the 1σ limit is 0.7 mags fainter, and the flux limit is 3×10^{-18} erg cm $^{-2}$ s $^{-1}$.

For the HDF additional V and I data were obtained with the UH8K camera at CFHT (Barger *et al.* 1998) on the nights of UT 1997 April 3–8. These comprise twenty-two 1200-sec I -band exposures (8.3 hrs) and thirty-three 1200-sec V -band exposures (11 hrs) under conditions of mixed transparency. Net image quality is $\sim 0''.8$ FWHM in I and $\sim 0''.9$ in V on these exposures. The UH8K V data were registered to the LRIS data and a noise-weighted addition was performed. The I -band data were calibrated using shallower images obtained under photometric conditions with the UH 2.2 m telescope. The corresponding 1σ limits for the combined HDF observations over a corrected $3''$ diameter aperture are 27.2 (B), 27.4 (V), and 25.8 (I), where B and V are on the Johnson system and I is Kron-Cousins. For SSA22 the corresponding limits are 27.8 (B), 27.5 (V), and 25.8 (I).

Two catalogs were next generated. The first was a narrow-band catalog of all objects selected to lie above a surface brightness of 27.9 mags/□'' (AB) in a $0''.8$ boxcar-smoothed narrow-band image, and above a 5σ limiting aperture magnitude $N(AB) = 25$ for the HDF and 25.7 for SSA22. B , V , and I magnitudes were measured for all these objects, and redshifts compiled from the literature (Songaila 1994; Steidel *et al.* 1996a; Cowie *et al.* 1996; Cohen *et al.* 1996; Lowenthal *et al.* 1997; Steidel *et al.* 1998) and from unpublished spectroscopy by our group, which may be found in the Hawaii Active Catalog of the HDF (Songaila *et al.* 1997). The combined narrow-band catalogs contain 1574 objects brighter than $N(AB) = 25$ of which 412 have spectroscopic identifications, and for SSA22 an additional 286 objects with $25 < N(AB) < 25.5$ of which only ten have spectroscopic identifications. A second V -selected catalog was generated consisting of all objects with surface brightnesses above 29.1 mags/□'' in the $0''.8$ smoothed V image and with $V < 25.7$ (the 5σ limit for the HDF). B , V , and $N(AB)$ magnitudes were measured for these objects, and redshifts were compiled. The V -selected catalog contains 2375 objects, of which 457 have spectroscopic IDs. Because the center of the narrow-band filter lies very close to the center of the V filter there is only a very small color difference term. In the subsequent discussion we use $N = N(AB) + 0.11 - 0.04(V - I)$ to correct for this. The magnitudes in the SSA22 field have also been corrected for a small amount of galactic extinction ($E_{B-V} = 0.05$) using a standard reddening law.

In Figs. 1a and 1b we show the LRIS fields of the narrow-band exposures – over a $380'' \times 275''$ region for the HDF (Fig. 1a) and over a $390'' \times 280''$ region for SSA22 (Fig. 1b). The catalog field corresponds to objects within the central $6'.0 \times 4'.2$ region, providing similar coverage to other $z > 4$ Ly α narrow-band surveys around quasars (*e.g.*, Hu & McMahon 1996) that will be discussed in later papers, or an area roughly $4.4\times$ the size of the HDF proper. Objects with observed equivalent widths in excess of 77 \AA in the narrow-band catalog are circled; objects which additionally have measured redshifts within this sample are circled with heavy borders (here, just the $z = 3.430$ object in the HDF found by Lowenthal *et al.* 1997 and shown in Fig. 1a). Image ghosts can be seen around the brightest objects in the fields but do not significantly change the sampling area or sensitivity limits. Figure 2a shows the corresponding regions for the Keck V -band images of the HDF (redshift identifications given in the annotations to the overlay in Fig. 2b) and SSA22 (Fig. 2c). In these images circles indicate the $V < 25.5$ objects which are red in $(B-V)$ and blue in $(V-I)$ ($(B-V) > 1.1$, $(V-I) < 1.6$). Again, objects encircled with heavy borders in each figure have measured redshifts, in addition to matching the specified color criteria. In the two fields eight of these objects are $z > 2.9$ galaxies (including one quasar), four are galaxies near $z \sim 0.3$ and 2 are stars. The HDF is richer in such objects than SSA22 by a factor of roughly 2.5, suggesting that there is substantial variation in the surface density of $z > 3$ objects from field to field for images with areas of this size.

3. Emission-Line Objects Selected by the Narrow-Band Filter

In Fig. 3 we plot $(V-N)$ vs N for the objects in the narrow-band selected catalog. The solid lines show the 3σ errors. The dashed line shows the $(V-N)$ color for objects which would have Ly α equivalent widths in excess of 77 \AA (that is, in which the flux in the narrow band is double that of the continuum). The vertical bar shows the expected $(V-N)$ range for objects with observed equivalent widths from 77 \AA to ∞ . The large solid box shows the Lowenthal *et al.* object. In the HDF there are five objects in the field with observed equivalent widths in excess of 77 \AA and with $N < 25$, and in SSA22 there are seven such objects with $N \leq 25.5$. The fluxes, equivalent widths, V magnitudes, and colors of the objects are summarized in Table 1. The equivalent widths of most of the objects are such that they are unlikely to be [O II] emitters since the rest frame [O II] equivalent width rarely exceeds 100 \AA (*e.g.*, Songaila *et al.* 1994), and indeed, for the one spectroscopically identified object the emission is due to Ly α , which is the only plausible alternate. We therefore consider these objects as the candidate sample of strong Ly α emitters and attempt to confirm this with other diagnostics.

In Fig. 4 we plot the locus of the $(V-I)$ vs $(B-V)$ colors for the narrow-band selected objects in the LRIS fields, and compare these to the color distribution of V -selected catalog objects in the HDF proper, and V -selected objects in the LRIS image of the SSA22 field. The objects that meet our equivalent width criterion and which are bright enough in the continuum for colors to be measured (Table 1) (*solid squares*) have predominantly red $(B-V)$ colors, but are blue (or close to flat-spectrum f_ν) in $(V-I)$ colors, as would be expected for high-redshift objects that are dominated by star formation (Cowie 1988; Songaila, Cowie, & Lilly 1990; Steidel *et al.* 1996a, 1996b; Lowenthal *et al.* 1997). These objects occupy the same region of the color-color diagram as objects seen in the tail of the color-color distribution for the HDF proper at bluer $(V-I)$ (or F602W – F814W) and red $(B-V)$ (Fig. 4, *top right panel*), and which correspond to high-redshift galaxies selected by color. As we shall demonstrate using the colors of HDF objects with known redshifts, these continuum colors can also distinguish redshift $z \sim 3.4$ objects from lower- z emitters. (We also note that the narrow-band catalog has a shallower slope in the Fig. 4 color-color diagrams for the HDF because the F602W filter is redder than the V -band used with LRIS.) The color selection criterion is therefore consistent with the interpretation that nearly all of the sample are Ly α emitters.

The redshift information also allows us to check the equivalent width selection procedure. In Fig. 5 we show $(V-N)$ vs redshift, with the redshift intervals matching the narrow-band filter band-pass indicated for emission from [O III] $\lambda 5007$ (at $z \sim 0.08$), [O II] $\lambda 3727$ (at $z \sim 0.45$), Mg II $\lambda 2800$ (at $z \sim 0.93$), and Ly α $\lambda 1216$ (at $z \sim 3.43$). These are the most prominent spectral features in most galaxies (cf., Songaila *et al.* 1994; Cowie *et al.* 1995a), with Mg II normally seen in absorption, and they are clearly seen in the color-redshift plot. The increasing width of the redshift interval corresponding to the narrow-band wavelengths at high redshifts is also seen. The scatter of points gives an idea of the real distribution of the signal strength of each feature, and it may also be seen that the high- z Ly α emitter, corresponding to the Lowenthal *et al.* object, does indeed have appreciably higher equivalent width than any of the [O II] emitters. We also note that other structures arise from additional spectral features (*e.g.*, the 4000 Å break and Fe II absorption lines) which add to the dispersion.

The color trends shown in Fig. 4 can also be examined in more detail by supplementing the measured colors for these objects with redshift information. In Fig. 6 we plot $(B-V)$ colors vs redshift for all galaxies in our V -selected catalog for which this information is available. It may be seen that applying a blue $(V-I)$ color criterion ($(V-I) < 1.6$) selects galaxies over a range of redshifts, extending at least to $z \sim 3.5$, but that within this subsample there are very definite trends in $(B-V)$ color with redshift. This function ($(B-V)$ vs redshift) remains double-valued out to about $z \sim 3$, with a progressive decrease (bluing)

in $(B-V)$ color as the 4000 Å Balmer break moves out of the B band to longer wavelengths in the observed frame. At higher redshifts the combination of the Lyman break and the depression of the continuum below Ly α due to increasing absorption by Ly α forest clouds leads to progressively redder observed $(B-V)$ colors, and $z > 3$ galaxies are easily distinguished. The data show that using the color criterion $(V-I) < 1.6$ and $(B-V) > 1.1$ will select primarily $z \gg 3$ galaxies, though a with a small admixture of low-redshift galaxies and stars.

In Fig. 7 we show how local continuum shape can be used to discriminate between the three classes of emission lines ([O II], [O III], and Ly α) that produce significant equivalent widths in the narrow band and hence to identify weaker Ly α emitters than would be picked out by the strong equivalent width criterion used previously. For the low-redshift [O III] lines the continuum is flat and $(B-V) < 0.4$ (*lower panel*). For the [O II] lines there is a strong discontinuity just redward of 3727 Å (*e.g.*, Lilly *et al.* 1995) which places $(B-V)$ in the 0.4 – 1.0 range. Finally, for the Ly α lines the strong discontinuity produced by the Ly α forest across the Ly α line places $(B-V) > 1.0$ (Cowie 1988; Madau *et al.* 1996).

We have divided the entire sample ($N(AB) < 25$ in the HDF, $N(AB) < 25.5$ in SSA22) in the same way in Figure 8. Here it can be seen that the $(B-V)$ selection chooses out the highest equivalent width objects with only one object falling into the $(B-V) < 1$ class having $(V-N) > 0.78$. As is illustrated in Fig. 8 a $(V-N) > 0.5$, $(B-V) > 1$ criterion should be effective in picking out emitters. However, weaker $(V-N)$ cuts become contaminated by error and color spread. The color-enhanced selection criterion therefore yields only a small number of additional objects over the simple strong equivalent width criterion.

4. Discussion

The strong equivalent width criterion gives ten strong Ly α emitters with flux $> 2 \times 10^{-17}$ erg cm $^{-2}$ s $^{-1}$ in the 46 \square' field coverage (about 800/ \square°) lying in the redshift range $z = 3.405 \rightarrow 3.470$, or roughly 13,000/unit z/\square° . Two of these objects — both lying in the SSA22 region — are completely undetected in the continuum at the 1 σ level of $V = 27.5$, while the remainder have V magnitudes ranging from 24.6 to 26.5 (Table 1). To a $V = 25.5$ magnitude limit a color criterion $(B-V) > 1.1$, $(V-I) < 1.6$ of the type discussed above gives 72 objects within the sample area when known low-redshift galaxies or stars are excluded. If we assume a rough z range of 3.1 \rightarrow 3.5, where the upper limits is determined by the passage of the forest through the middle of the V band, this selection also corresponds to a surface density of 13,000/unit z/\square° . While the number is quite uncertain because of the small number statistics, the choice of magnitude limit, and the possibility of redshift clustering, there are

comparable numbers of strong Ly α emitters and color-selected galaxies at these flux selection limits. This is consistent with the spectroscopic properties of the color-selected objects with measured high redshifts, and it appears that Ly α emission is quite common in the high-redshift objects. In addition, there appear to be numbers of bare Ly α emitters where the continuum is undetectable, which balances to some extent the presence of color-selected objects without strong emission.

In the absence of extinction and with the assumption that the Ly α emission is produced by photoionization by stars, the conversion from Ly α luminosity to star formation rate is $1 M_{\odot} \text{ yr}^{-1} \rightarrow 10^{42} \text{ erg s}^{-1}$ in the Ly α line, where we have used Kennicutt's (1983) relation between the star formation rate and H α luminosity and the Case B Ly α /H α = 8.7 (Brocklehurst 1971). Because of the effects of extinction the Ly α luminosity is likely to underestimate the SFR, while if some portion of the Ly α luminosity is powered by AGN we will overestimate the SFR. The size of these effects is not easy to estimate, though the rest-frame equivalent widths of the lines (Table 1) imply that if the objects are photoionized that extinction cannot reduce the line luminosities by more than a factor of about two before reasonable theoretical upper bounds on the equivalent width (Charlot & Fall 1993) are exceeded. We also note that in the spectra obtained to date of the SSA22 emitters (Hu *et al.* 1998) there is little sign of the C IV line which might indicate AGN activity.

Proceeding therefore under the assumption that the line is photoionized by stars and neglecting extinction, we find maximum star formation rates of just under $10 h_{50}^{-2} M_{\odot} \text{ yr}^{-1}$ for $q_0 = 0.5$, which are very similar to those seen at lower z (Cowie *et al.* 1997) and those inferred from the continuum light of color-selected objects at these redshifts (Steidel *et al.* 1998). In Fig. 9 we show the Ly α luminosity function constructed for $H_0 = 65 \text{ km s}^{-1} \text{ Mpc}^{-1}$ and $q_0 = 0.5$. In the absence of extinction this may be directly converted to an \dot{M} distribution using the $L(\text{Ly}\alpha)$ – \dot{M} relation. The \dot{M} function is quite similar to that seen at $z = 1$ (Cowie *et al.* 1997) within the large statistical uncertainties and modulo the different methodologies used (UV fluxes vs Ly α luminosities). It is more probable that \dot{M} is underestimated at the high redshift because extinction must have a larger effect on the Ly α line than on the continuum. Integrating through the \dot{M} function we find a star formation density of $0.01 M_{\odot} \text{ Mpc}^{-3} \text{ yr}^{-1}$, which is quite similar to that inferred from color arguments (*e.g.*, Madau *et al.* 1996, Mobasher & Mazzei 1997). Again, it must be emphasized that this is an extreme lower limit since we neglect extinction.

We thank Boris Shnapir for assistance in the design and fabrication of the narrow-band filter, Bob Williams and Richard Ellis for comments on an earlier draft of this paper, and Tom Bida and Bob Goodrich for their assistance in obtaining the observations, which would not have been possible without the LRIS spectrograph of Judy Cohen and Bev Oke. Support for

this work was provided by the State of Hawaii and by NASA through grants number GO-5975.01-94A, GO-06222.01-95A, and AR-06377.06-94A from the Space Telescope Science Institute, which is operated by AURA, Inc., under NASA contract NAS 5-26555. E.M.H. would also like to gratefully acknowledge a University Research Council Seed Money grant.

REFERENCES

- Barger, A. *et al.* 1998, in preparation
- Brocklehurst, M. 1971, MNRAS, 153, 471
- Charlot, S., & Fall, S. M. 1993, ApJ, 415, 580
- Cohen, J. G., Cowie, L. L., Hogg, D. W., Songaila, A., Blandford, R., Hu, E. M., & Shopbell, P. 1996, ApJ, 471, L5, astro-ph/9608121
- Cowie, L. L. 1988, in *The Post-Recombination Universe*, edited by N. Kaiser and A. N. Lazenby (Kluwer, Dordrecht), p. 1
- Cowie, L. L., Gardner, J. P., Hu, E. M., Songaila, A., Hodapp, K.-W., & Wainscoat, R. J. 1994, ApJ, 434, 114
- Cowie, L. L., Hu, E. M., & Songaila, A. 1995a, Nature, 377, 603, astro-ph/9510045
- Cowie, L. L., Hu, E. M., & Songaila, A. 1995b, AJ, 110, 1576, astro-ph/9507055
- Cowie, L. L., Hu, E. M., Songaila, A., & Egami, E. 1997, ApJ, 481, L9, astro-ph/9702235
- Cowie, L. L., Songaila, A., & Hu, E. M. 1991, Nature, 354, 460
- Cowie, L. L., Songaila, A., Hu, E. M., & Cohen, J. G. 1996, AJ, 112, 839, astro-ph/9606079
- Djorgovski, S., Spinrad, H., McCarthy, P., & Strauss, M. 1985, ApJ, 299, L1
- Djorgovski, S. G., Pahre, M. A., Bechtold, J., & Elston, R. 1996, Nature, 382, 234, astro-ph/9511040
- Francis, P. J., Woodgate, B. E., & Danks, A. C. 1997, ApJ, 482, L25, astro-ph/9703178
- Francis, P. J., Woodgate, B. E., Warren, S. J., Møller, P., Mazzolini, M., Bunker, A. J., Lowenthal, J. D., Williams, T. B., Minezaki, T., Kobayashi, Y., & Yoshii, Y. 1996, ApJ, 457, 490, astro-ph/9511040
- Hu, E. M., Cowie, L. L., & McMahon, R. G. 1998, in preparation
- Hu, E. M., & McMahon, R. G. 1996, Nature, 382, 231, astro-ph/9606135
- Hu, E. M., McMahon, R. G., & Egami, E. 1996, ApJ, 459, L53, astro-ph/9512165
- Hu, E. M., McMahon, R. G., & Egami, E. 1997, in *HST and the High Redshift Universe*, edited by N. Tanvir, A. Aragón-Salamanca, and J. Wall (World Scientific, Singapore), p. 91, astro-ph/9609188
- Kennicutt, R. C., Jr. 1983, ApJ, 272, 54
- Kennicutt, R. C., Jr. 1992, ApJ, 388, 310
- Landolt, A. U. 1992, AJ, 104, 340

- Lilly, S. J., LeFèvre, O., Crampton, D., Hammer, F., & Tresse, L. 1995, *ApJ*, 460, L1, astro-ph/9507010
- Lowenthal, J. D., Koo, D. C., Guzmán, R., Gallego, J., Phillips, A. C., Faber, S. M., Vogt, N. P., Illingworth, G. D., & Gronwell, C. 1997, *ApJ*, 481, 673, astro-ph/9703093
- Macchetto, F., Lipari, S., Giavalisco, M., Turnshek, D. A., & Sparks, W. B. 1993, *ApJ*, 404, 511
- Madau, P., Ferguson, H. C., Dickinson, M. E., Giavalisco, M., Steidel, C. C., & Fruchter, A. 1996, *MNRAS*, 283, 1388, astro-ph/9607172
- Massey, P., Strobel, K., Barnes, J. V., & Anderson, E. 1988, *ApJ*, 328, 315
- Mobasher, B., & Mazzei, P. 1997, *MNRAS*, submitted
- Oke, J. B., Cohen, J. G., Carr, M., Cromer, J., Dingizian, A., Harris, F. H., Labrecque, S., Luciano, R., Schaal, W., Epps, H., & Miller, J. 1995, *PASP*, 107, 375
- Pascarelle, S. M., Windhorst, R. A., Keel, W. C., & Odewahn, S. C. 1996, *Nature*, 383, 45
- Petitjean, P., Pécontal, E., Valls-Gabaud, D., & Charlot, S. 1996, *Nature*, 380, 411, astro-ph/9603088
- Pritchett, C. J. 1994, *PASP*, 106, 1052
- Songaila, A. 1997, (<http://www.ifa.hawaii.edu/~cowie/tts/tts.html>) [Hawaii Active Catalog of the Hubble Deep Field] (20 February 1997)
- Songaila, A., Cowie, L. L., Hu, E. M., & Gardner, J. P. 1994, *ApJS*, 94, 461
- Songaila, A., Cowie, L. L., & Lilly, S. J. 1990, *ApJ*, 348, 371
- Steidel, C. C., Adelberger, K., Dickinson, M., Giavalisco, M., Pettini, M., & Kellogg, M. 1998, *ApJ*, (in press), astro-ph/9708125
- Steidel, C. C., Giavalisco, M., Dickinson, M., & Adelberger, K. L. 1996a, *AJ*, 112, 352, astro-ph/9604140
- Steidel, C. C., Giavalisco, M., Pettini, M., Dickinson, M., & Adelberger, K. L. 1996b, *ApJ*, 462, L17, astro-ph/9602024
- Williams, R. E. *et al.* 1996, *AJ*, 112, 1335, astro-ph/9607174

Table 1. Properties of Strong Emitters

ID	Flux (erg cm ⁻² s ⁻¹)	W _λ (observed) (Å)	V	(V – I)	(B – V)	z
HDF, N < 25						
HDF–LA1	8.0 (–17)	140	24.6	0.9	1.1	...
HDF–LA2	6.1 (–17)	135	24.8	0.5	1.4	...
HDF–LA3	5.2 (–17)	250	25.7	0.0	2.2	...
HDF–LA4	3.2 (–17)	115	25.4	1.6	1.9	3.430 ^a
HDF–LA5	2.4 (–17)	250	26.5	0.2	1.1	...
SSA22, N < 25.5						
SSA22–LA1	6.7 (–17)	325	25.7	0.8	2.4	3.455 ^b
SSA22–LA2	5.2 (–17)	230	25.6	0.8	1.6	3.460 ^b
SSA22–LA3	3.8 (–17)	> 845	–28.0 ^c	3.450 ^b
SSA22–LA4	2.5 (–17)	140	25.9	0.2	1.3	...
SSA22–LA5	2.0 (–17)	> 405	–28.7 ^c
SSA22–LA6	1.5 (–17)	115	26.2	0.4	1.0	...
SSA22–LA7	1.2 (–17)	90	26.2	2.2	1.2	0.442 ^b

^aLowenthal *et al.* 1997

^bHu *et al.* 1998, in preparation

^cA negative V magnitude here indicates that there is a negative flux in the aperture. The 1 σ limits on V are 27.4 (HDF) and 27.5 (SSA22).

Fig. 1a.— Narrow-band image of the HDF and surrounding field. The displayed field of view shows a $380'' \times 275''$ region from a 2-hr exposure taken with LRIS on the Keck II 10-m telescope through the 5390/77 Å narrow-band filter in the collimated beam. The composite image quality is $\sim 0''.7$ FWHM, with a 1σ limiting AB magnitude of 26.8 over a $3''$ diameter aperture, corrected to a total magnitude following Cowie *et al.* (1994), and with a corresponding 1σ flux of 6×10^{-18} erg cm $^{-2}$ s $^{-1}$ over the same aperture. Circled items indicate field objects with narrow-band equivalent widths in excess of 77 Å in the observed frame, and which also fall within the central $6'.0 \times 4'.2$ region used for the narrow-band catalog (including objects brighter than the 5σ limiting magnitude of 25). The heavily circled object is the one catalogued narrow-band object which lies within the HDF proper. (The LRIS field displayed covers an area 4.4 times larger than the HDF field). This has a redshift identification by Lowenthal *et al.* (1997) of $z = 3.430$ (object id hd2-0698-1297), in agreement with the Ly α selection of the filter. This is also the only object among currently reported galaxies lying within the HDF with a redshift that would place Ly α emission within the filter bandpass; however, we note that no information about object emission-line redshifts in the selected bandpass was available at the time the filter was designed. Circled overlays correspond to a $4''.6$ diameter aperture. Most of the indicated emission-line objects are more compact than the object identified by Lowenthal *et al.*, as was generally true of the other high-redshift objects discussed in that paper. This object also lies at the lower end of our equivalent width selection criterion.

Fig. 1b.— Narrow-band image of the SSA22 field. The field of view seen in this image is $390'' \times 280''$, and reaches a 1σ flux of 3×10^{-18} erg cm $^{-2}$ s $^{-1}$ over a $3''$ diameter aperture for the 5-hr exposure. The circled items correspond to objects whose emission is in excess of an equivalent width of 77 Å for $N(AB) < 25.5$.

Fig. 2a.— The corresponding V -band image of the HDF, comprising 0.6 hrs on Keck II (LRIS) combined with 11 hrs on CFHT with the UH8K mosaic CCD camera. The 1σ (Johnson) V limit over a corrected $3''$ diameter aperture is 27.4. Encircled objects are selected from $V < 25.5$ objects which have red $(B-V)$ colors ($(B-V) \geq 1.1$) and blue $(V-I)$ colors ($(V-I) \leq 1.6$), many of which should correspond to high-redshift galaxies. Again, objects with heavy circles indicate galaxies which meet the selection criteria, and also have measured redshifts, given in Fig. 2b. Four of the remaining color-selected objects lie in the HDF proper. Of these, one (hd2_0853_0319) has a tentative redshift of $z = 3.35$ from Lowenthal *et al.* 1997.

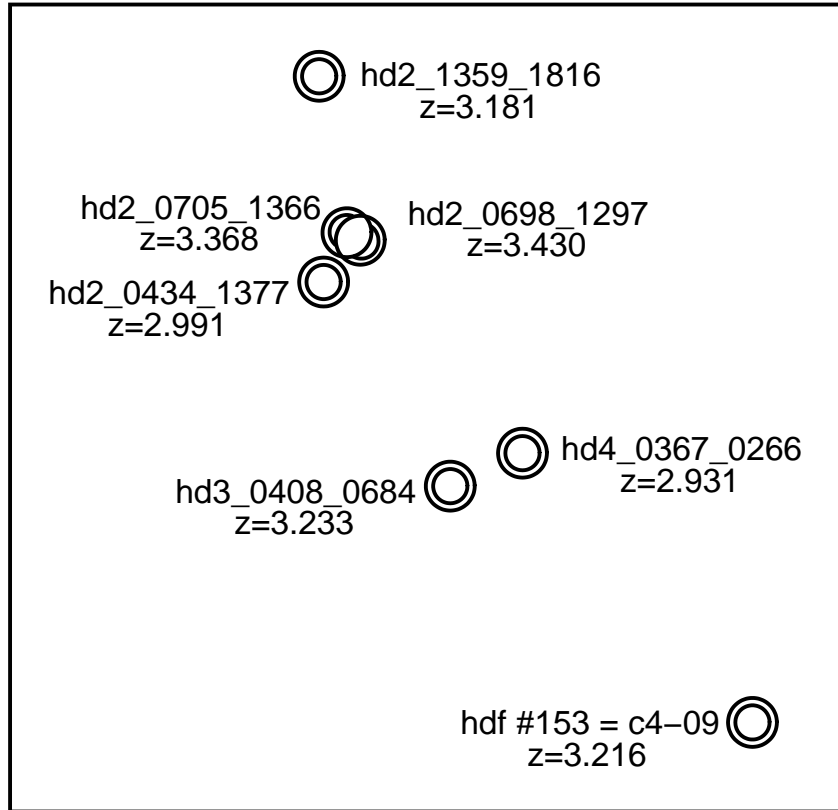


Fig. 2b.— Identifications of high-redshift galaxies in the HDF which have been spectroscopically identified in Lowenthal *et al.* 1997, in the Hawaii Active Catalog, or in Steidel *et al.* 1996a.

Fig. 2c.— The V -band image of SSA22, with circled objects showing the color selection for high-redshift galaxies applied in Fig. 2a, and with those galaxies with measured redshifts (known in the literature prior to our spectroscopic follow-up) indicated with heavy circles. The 1σ V limit is 27.5.

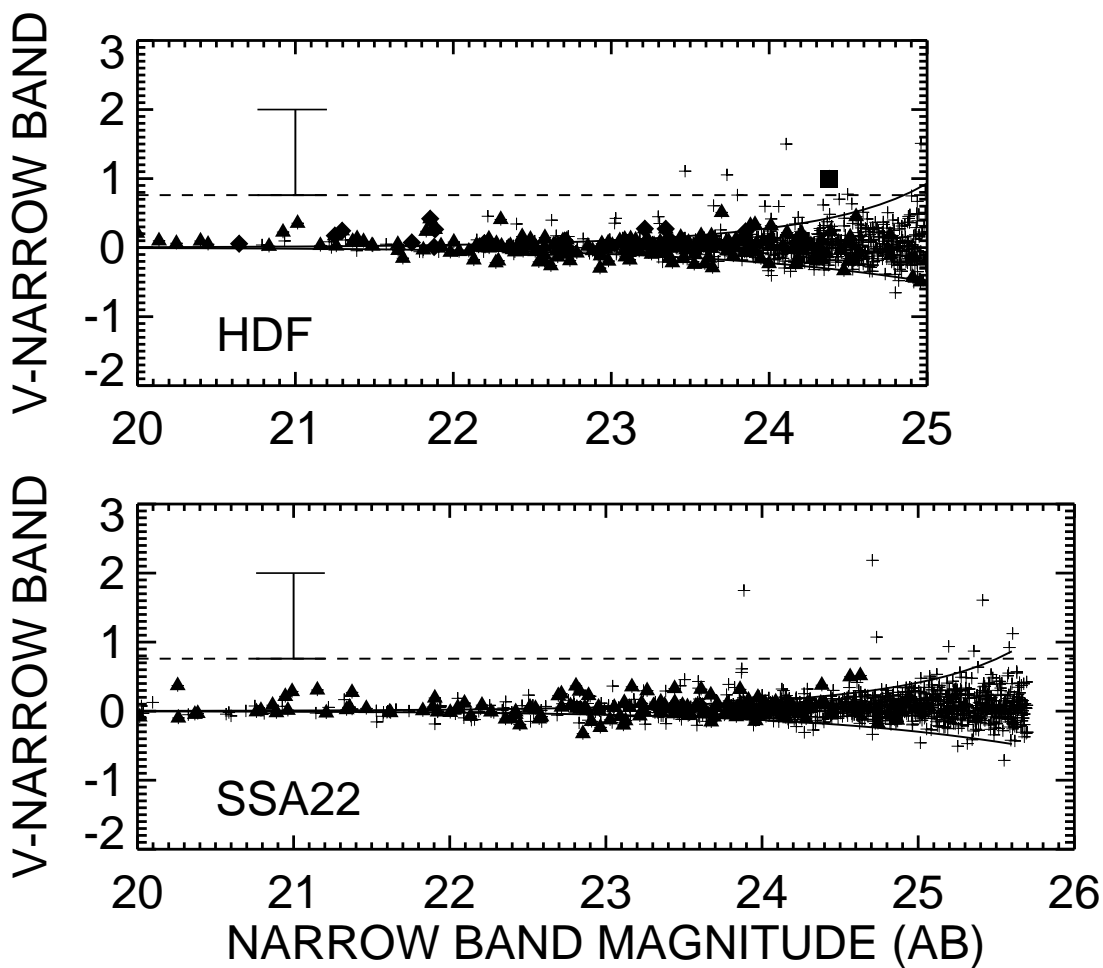


Fig. 3.— The distribution of emission-line excess ($V-N$) vs. N for objects (pluses) in the narrow-band catalogues for the HDF and SSA22. The solid lines show the distribution of 3σ errors. The solid box shows the Lowenthal *et al.* $z = 3.430$ object, the diamonds objects where $[\text{O II}] 3727$ falls in the filter bandpass, and the triangles other objects with measured redshifts. The dashed line shows the ($V-N$) color corresponding to an equivalent width of 77 \AA and the vertical bar shows the expected ($V-N$) distribution for objects with observed equivalent widths ranging from 77 \AA to ∞ .

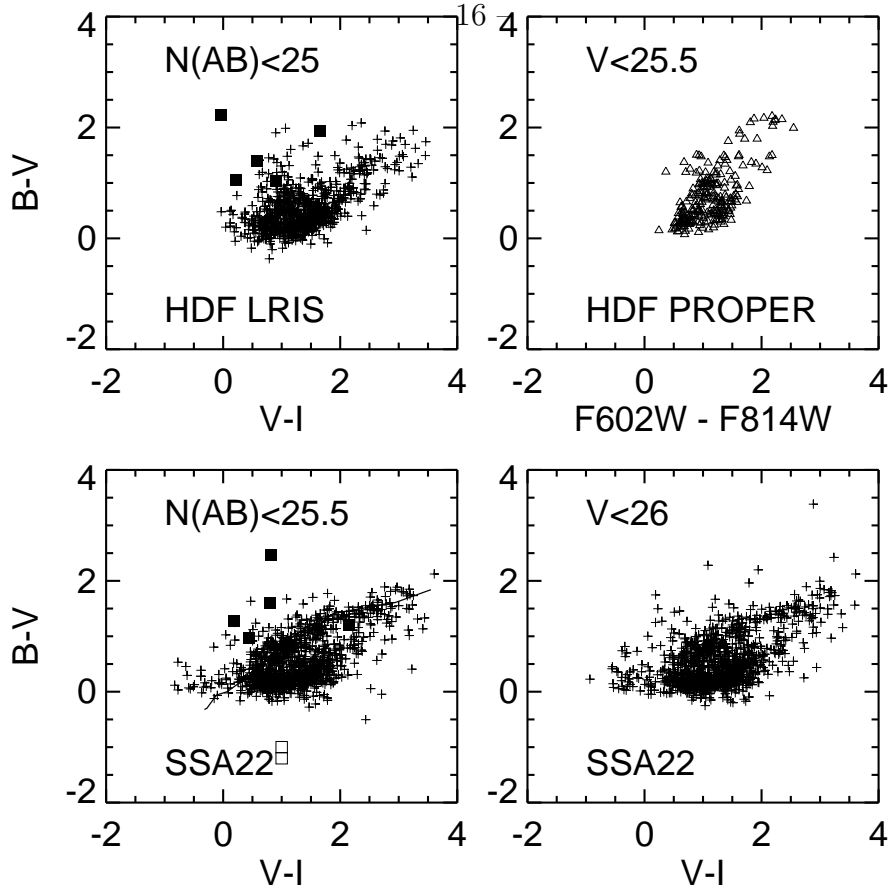


Fig. 4.— $(B-V)$ vs $(V-I)$ color-color plots for objects in the HDF and SSA22 fields selected from the narrow-band and V -band catalogues. The left-hand plots show the color distributions of objects in the narrow-band catalogues ($N(AB) < 25$ for the LRIS HDF field and $N(AB) < 25.5$ for the LRIS SSA22 field). The colors of emission-line objects in these magnitude-selected catalogues with equivalent widths in excess of 77 \AA in the observed frame are indicated with squares, and may be seen to lie at red ($B-V$) and blue ($V-I$) colors. Two of the strong emission-line objects in the SSA22 field have continua which are either undetected or too faint to provide color measurements (Table 1). They are indicated schematically by open squares placed at nominal color positions. The slightly higher density of stars in the SSA22 field ($b^{II} \sim -44^\circ$) compared with the HDF ($b^{II} \sim +55^\circ$) may be seen in the more populated star track (*solid line*) which approaches the blue end of the high- z galaxy color distribution. The right-hand plots show the color-distribution of objects from our V -selected catalogues ($V < 25.5$ for the HDF and $V < 26$ for SSA22). For the HDF, the available *HST* filter measurements provide a tighter color distribution, and here we have elected to use (F602W–F814W) in place of $(V-I)$ and (F450W–F602W) in place of $(B-V)$, with the $V < 25.5$ sample restricted to the HDF proper (about a quarter of the size of the larger LRIS field). These points are shown as open triangles. The steeper slope of this color distribution is a reflection of the different wavelength centers (*e.g.*, F602W vs V) used for the abscissa.

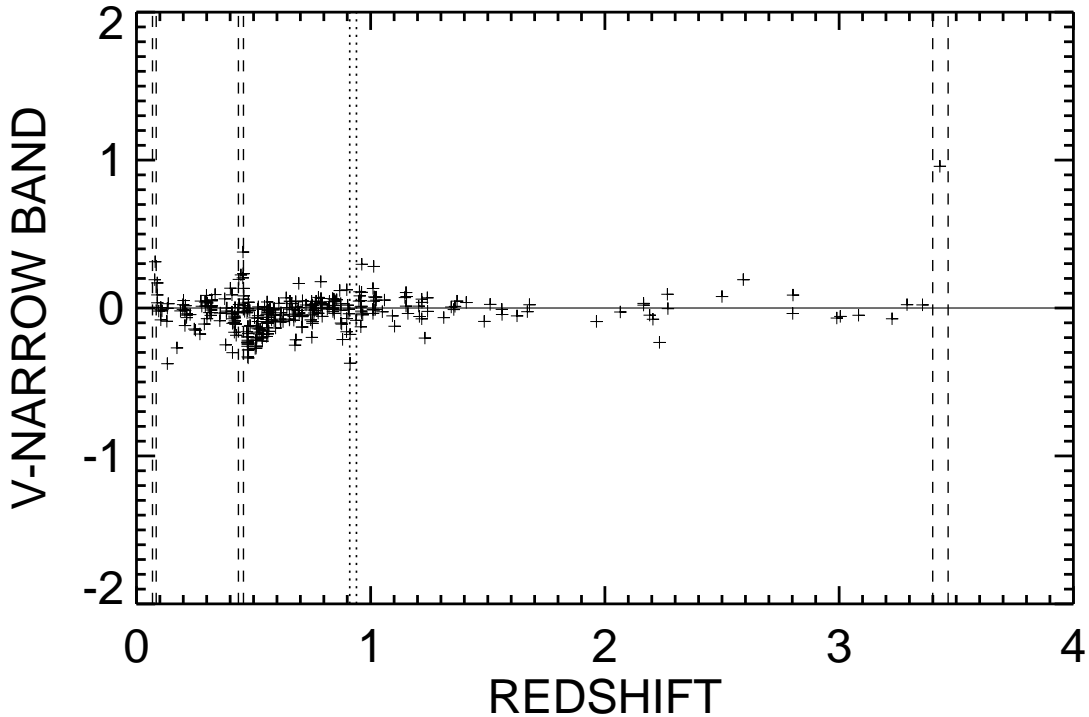


Fig. 5.— Excess emission in narrow-band over V -band vs redshift for objects in the HDF and SSA22 fields. Objects with spectroscopic identifications in the literature (Lowenthal *et al.* 1997; Cohen *et al.* 1997; Songaila 1997 HDF Active Catalog web page; Steidel *et al.* 1996a), over the HDF and SSA22 fields sampled by the LRIS deep imaging fields are shown here. The positions and redshift ranges corresponding to features such as Mg II (*dotted lines*) and $[\text{O III}]$, $[\text{O II}]$, and $\text{Ly}\alpha$ (*dashed lines*) falling within the filter bandpass are indicated. The structure of the continuum near the $[\text{O II}]$ feature may be seen reflected in both the ‘dip’ and dispersion of points in this region, and it may also be seen that emission-line objects in $[\text{O II}]$ and a few $[\text{O III}]$ emitters may be detected. Underlying continuum features can also increase the dispersion of these points in different redshift regions. At higher redshifts a correspondingly wider redshift region is sampled by the filter bandpass. Redshifts used only include values known at the time of the imaging observations, and do not include follow-up spectroscopic confirmations of candidate $\text{Ly}\alpha$ emitters, which will be described in Hu *et al.* (1998).

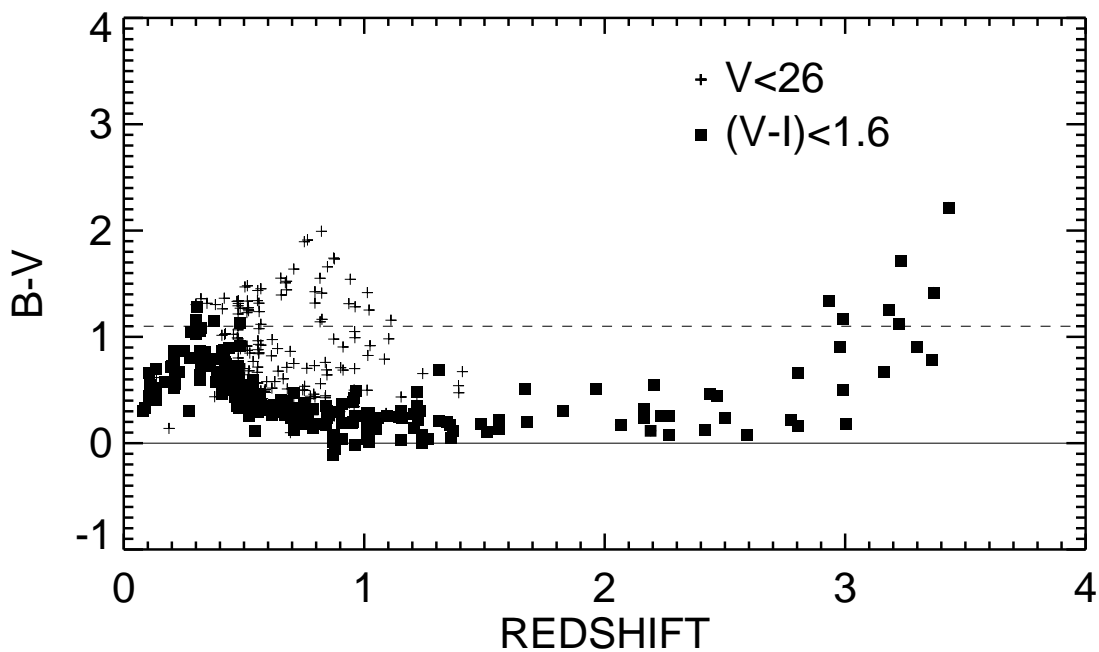


Fig. 6.— $(B-V)$ vs redshift for SSA22 and the HDF. For objects with known redshifts in these two fields, the $V < 26$ sample (*pluses*) is divided according to $(V-I)$ color. For those objects which are relatively blue in $(V-I)$ colors [$(V-I) < 1.6$] (*filled squares*) a clear trend in $(B-V)$ color with redshift may be seen, corresponding to passage of continuum break features through the reference bandpasses. At high redshifts ($z \gtrsim 2.9$) star-forming galaxies, which will have flat $(V-I)$ spectra, appear extremely red in $(B-V)$, and may be selected by their color breaks. A dashed reference line at $(B-V)$ corresponds to our $(B-V)$ color selection.

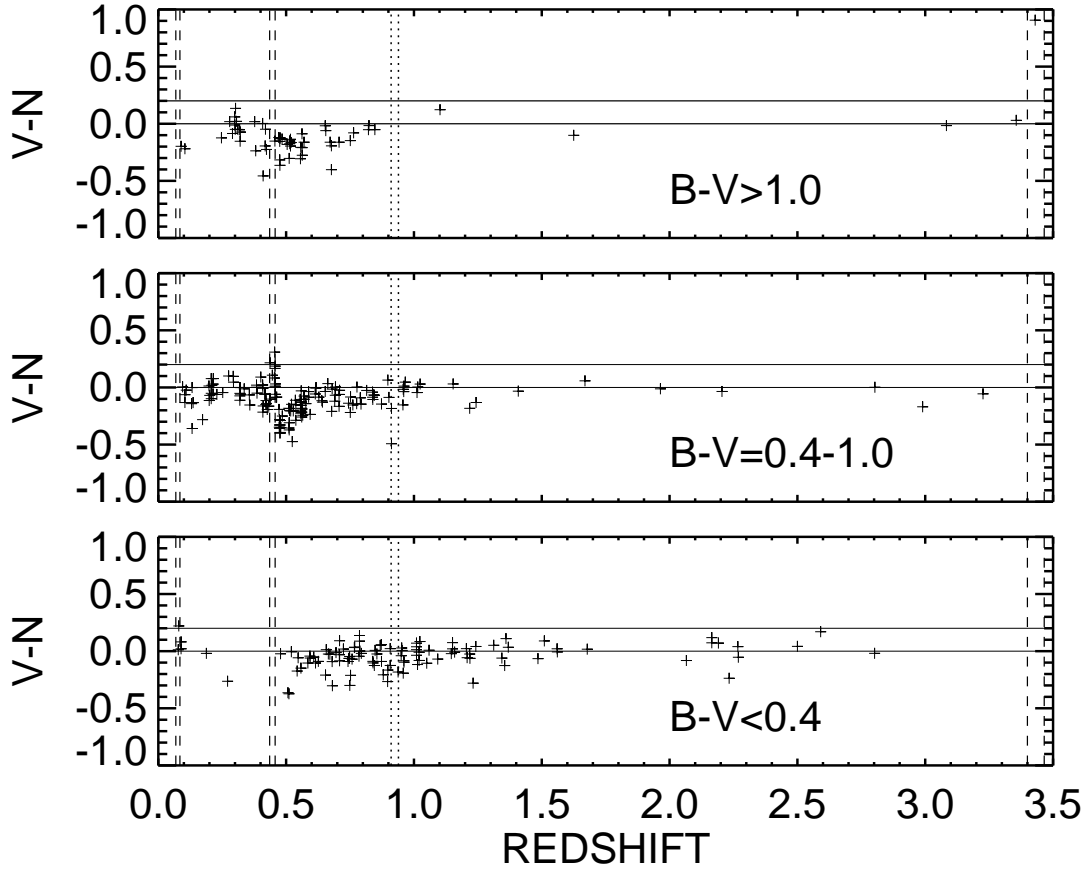


Fig. 7.— $(V-N)$ vs redshift for objects with $N(AB) < 24.5$ in three $(B-V)$ color subsamples. The data are grouped according to $(B-V)$ color, and illustrate the color trends with redshift of Fig. 6, which demonstrates that it is possible to discriminate between classes of emitters using color data, and hence to identify weaker $\text{Ly}\alpha$ emitters than would be possible with a strong equivalent width criterion. The solid lines show objects with $(V-N) > 0.2$. For $(B-V) > 1.0$ the identified emission-line object corresponds to $\text{Ly}\alpha$ at $z \sim 3.4$. In the intermediate $0.4 < (B-V) < 1.0$ color range $[\text{O II}]$ emission-line objects are selected. At $(B-V) < 0.4$ the narrow-band excess objects correspond to $[\text{O III}]$ emitters.

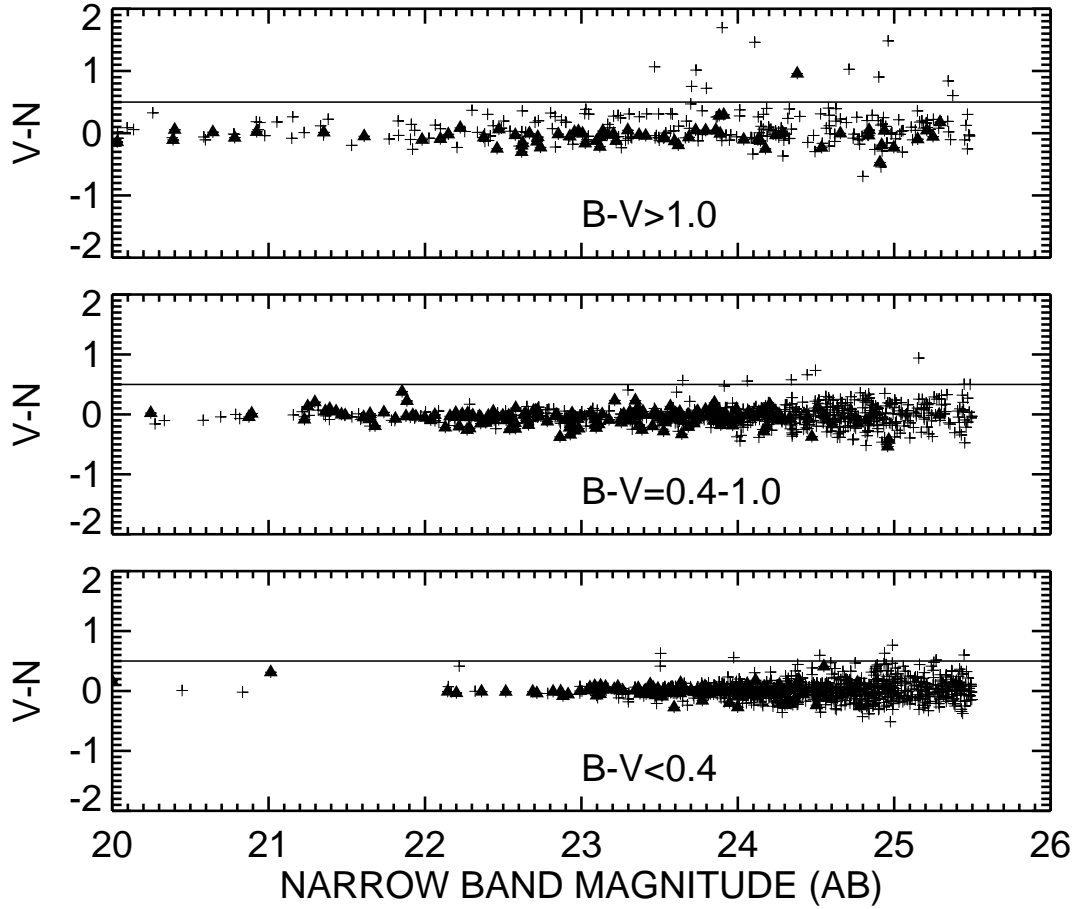


Fig. 8.— $(V-N)$ vs N for $N(AB) < 25$ in the HDF and $N(AB) < 25.5$ in SSA22 divided by $(B-V)$ color into three bins. Objects with known redshifts are marked with triangles. The dividing line in $(V-N)$ is set at 0.5.

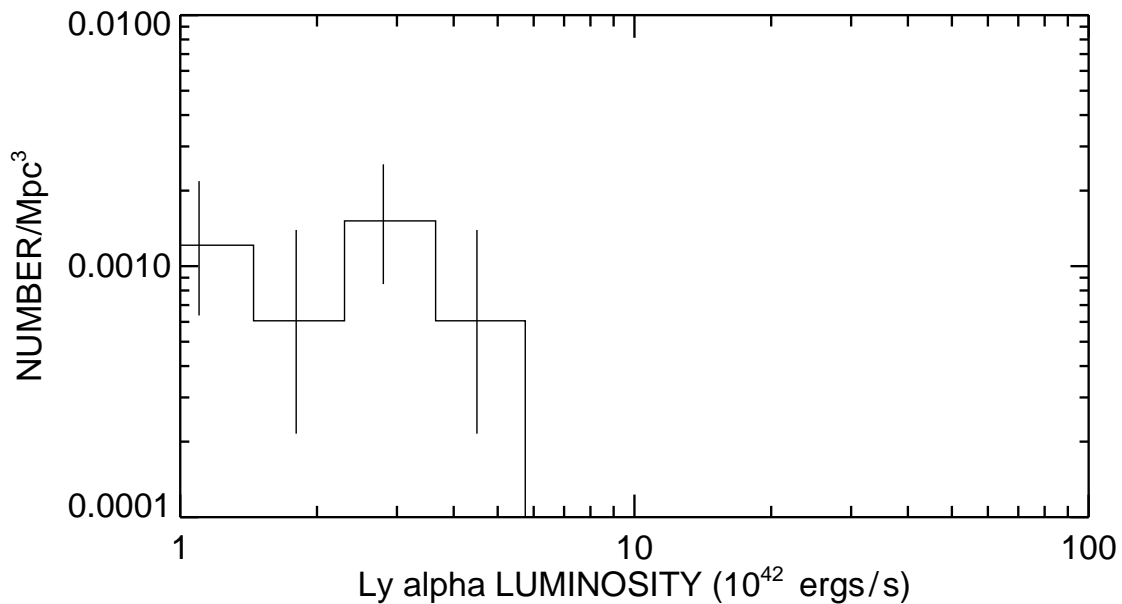


Fig. 9.— Distribution of Ly α emission vs Ly α luminosity for the strong equivalent width emission-line objects in the SSA22 and HDF LRIS fields. The horizontal axis may be converted to star formation rate in the absence of extinction and assuming that the Ly α is produced by photoionization, whence $10^{42} \text{ erg s}^{-1} \approx 1 M_{\odot} \text{ yr}^{-1}$. The errors are $\pm 1 \sigma$ based on the number of objects in each bin. See text for a more extensive discussion.

This figure "Fig1a.gif" is available in "gif" format from:

<http://arxiv.org/ps/astro-ph/9801003v1>

This figure "Fig1b.gif" is available in "gif" format from:

<http://arxiv.org/ps/astro-ph/9801003v1>

This figure "Fig2a.gif" is available in "gif" format from:

<http://arxiv.org/ps/astro-ph/9801003v1>

This figure "Fig2c.gif" is available in "gif" format from:

<http://arxiv.org/ps/astro-ph/9801003v1>